LETTER

doi:10.1038/nature25773

Phase-plate cryo-EM structure of a biased agonist-bound human GLP-1 receptor-Gs complex

Yi-Lynn Liang[1]*, Maryam Khoshouei[2]*, Alisa Glukhova[1]*, Sebastian G. B. Furness[1], Peishen Zhao[1], Lachlan Clydesdale[1], Cassandra Koole[1], Tin T. Truong[1], David M. Thal[1], Saifei Lei[3,4], Mazdak Radjainia[1,5], Radostin Danev[2], Wolfgang Baumeister[2], Ming-Wei Wang[3,4,6], Laurence J. Miller[1,7], Arthur Christopoulos[1], Patrick M. Sexton[1,6] & Denise Wootten[1]

The class B glucagon-like peptide-1 (GLP-1) G protein-coupled receptor is a major target for the treatment of type 2 diabetes and obesity[1]. Endogenous and mimetic GLP-1 peptides exhibit biased agonism—a difference in functional selectivity—that may provide improved therapeutic outcomes[1]. Here we describe the structure of the human GLP-1 receptor in complex with the G protein-biased peptide exendin-P5 and a $G\alpha_s$ heterotrimer, determined at a global resolution of 3.3 Å. At the extracellular surface, the organization of extracellular loop 3 and proximal transmembrane segments differs between our exendin-P5-bound structure and previous GLP-1-bound GLP-1 receptor structure[2]. At the intracellular face, there was a six-degree difference in the angle of the Gαs–α5 helix engagement between structures, which was propagated across the G protein heterotrimer. In addition, the structures differed in the rate and extent of conformational reorganization of the $G\alpha_s$ protein. Our structure provides insights into the molecular basis of biased agonism.

The GLP-1R, a class B G protein-coupled receptor (GPCR), is a key incretin hormone receptor and an important target for the development of therapies for the treatment of type 2 diabetes and obesity[1]. Biased agonism is commonly observed at the GLP-1R[3–5], and exendin-P5 (ExP5) has been identified as a potent G protein-biased selective agonist of GLP-1R, with diminished coupling to β-arrestins[6] and a unique *in vivo* profile in animal models of diabetes[6]. The prevalence of GLP-1R biased agonism and its therapeutic implications make understanding of the phenomenon at molecular and structural levels crucial for the rational design of novel ligands.

Like all class B GPCRs, the GLP-1R contains a large extracellular N-terminal domain (NTD) and a seven-transmembrane helix bundle, with peptide binding spanning both domains; the NTD interaction positions the peptide N terminus within the receptor core to facilitate receptor activation[7]. Clinically used therapeutic agents, including exendin-4, contain an N-terminal sequence that is relatively conserved with that of the native peptide, GLP-1[8]. Notably, ExP5 shares a common C terminus with exendin-4, but possesses a unique N-terminal domain (Extended Data Fig. 1a) that interacts with the GLP-1R transmembrane core to promote receptor activation.

Cryo-electron microscopy (cryo-EM) has enabled researchers to determine the structures of GPCR complexes without the need to extensively modify the receptor[2,9]. A 4.1 Å full-length active structure of a wild-type rabbit GLP-1R was solved in complex with GLP-1 and heterotrimeric G_s protein[2]. In addition, the full-length active structure of the calcitonin receptor (CTR) was solved to a similar global resolution in complex with a peptide agonist and G_s protein[9] using phase contrast cryo-EM[10–12]. Here, we used Volta phase plate cryo-EM to determine the structure of an active state, human GLP-1R bound to ExP5 in complex with a heterotrimeric G_s protein. The structure provides insights into the binding of ExP5 to the GLP-1R, with implications for receptor activation, G protein coupling and signalling for class B GPCRs.

To form an active, G protein-coupled complex, the GLP-1R was co-expressed with $G\alpha_s$, His-Gβ1, and Gγ2 in *Trichoplusia ni* (Tni) insect cells and stimulated with an excess of ExP5 in the presence of apyrase and the nanobody Nb35, which bridges the G protein α- and βγ-subunits. A dominant-negative $G\alpha_s$ was used to enable the formation of a complex with improved stability. We characterized and purified the complex as described for the CTR[9] (Extended Data Figs 1b, 2a).

Following imaging and initial 2D classification (Extended Data Fig. 2b, c), 3D classification revealed that the majority of the complex had stable features. The exception was the $G\alpha_s$ α-helical domain, the density of which was averaged out at higher resolution because it had substantial flexibility despite occupying a single predominant orientation (Fig. 1a). We used 184,672 particle projections to obtain a cryo-EM density map with nominal global resolution of 3.3 Å (Fig. 1a; Extended Data Fig. 2b).

An atomic resolution structure of the ExP5–GLP-1R–$G\alpha_s$ heterotrimeric G protein complex was built into the map and refined to reveal global features similar to those observed in other class B GPCR structures[2,9,13–15]. Side chains of the majority of amino acid residues are clearly identifiable in the peptide, all of the transmembrane helices and the subunits of the G protein (Extended Data Fig. 3). Although linker region density between the NTD and the transmembrane core was visible in the cryo-EM map, it was less well-resolved than other receptor domains, suggesting substantial flexibility in the ExP5 bound state. Continuous density was observed for helix 8 (H8) and all intracellular and extracellular loops (ICLs and ECLs, respectively), with the exception of ICL3, which was not modelled. In addition, the cryo-EM map was poor for a region of four ECL3 residues (372–375) and therefore only the protein backbone was modelled in this region.

Within the NTD there was discontinuous density in the backbone for some regions. As such, the NTD structure bound to exendin(9–39)[16] was used to perform a rigid body fit into the density. N-terminal residues 24–30 and residues beyond E423 at the receptor C terminus were not resolved. The G protein was well resolved, allowing modelling of all G protein components (with the exception of the Gαs α-helical domain).

The extracellular NTD conformation differs between the three agonist-bound $G\alpha_s$ heterotrimer class B GPCR structures (Extended Data Fig. 4a–c). Whereas multiple NTD conformations were evident for the CTR[9], a single predominant conformation was stabilized in both GLP-1R structures[2]. However, there were subtle differences in the relative positioning of the N terminus relative to the transmembrane

[1]Drug Discovery Biology and Department of Pharmacology, Monash Institute of Pharmaceutical Sciences, Monash University, Parkville 3052, Victoria, Australia. [2]Department of Molecular Structural Biology, Max Planck Institute of Biochemistry, 82152 Martinsried, Germany. [3]University of Chinese Academy of Sciences, 19A Yuquan Road, Beijing 100049, China. [4]The National Center for Drug Screening and CAS Key Laboratory of Receptor Research, Shanghai Institute of Materia Medica, Chinese Academy of Sciences, Shanghai 201203, China. [5]FEI, 5651 GG Eindhoven, The Netherlands. [6]School of Pharmacy, Fudan University, Shanghai 201203, China. [7]Department of Molecular Pharmacology and Experimental Therapeutics, Mayo Clinic, Scottsdale, Arizona 85259, USA.
*These authors contributed equally to this work.

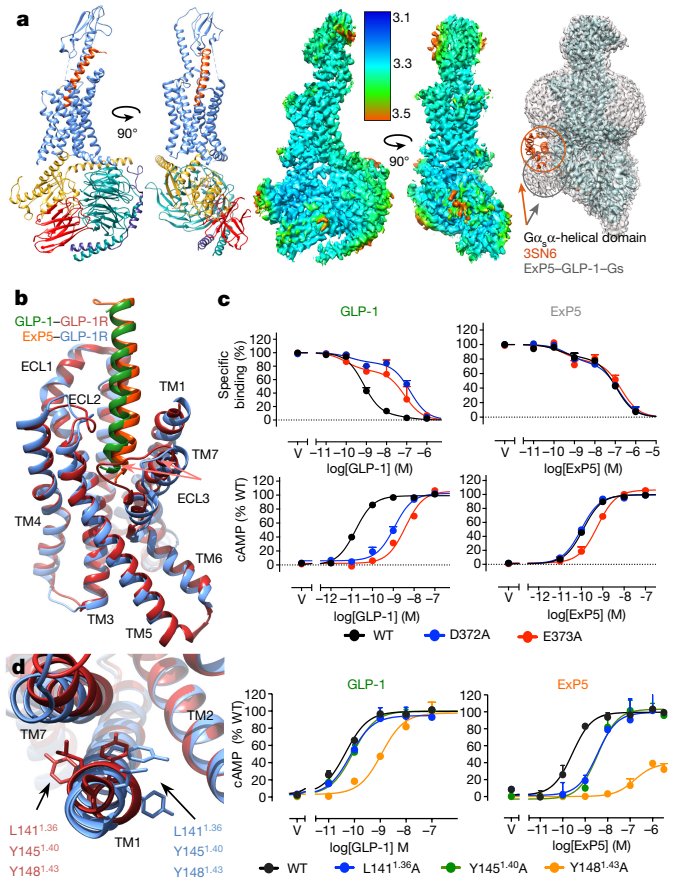

Figure 1 | The ExP5–GLP-1R–Gs cryo-EM structure reveals molecular details linked to GLP-1R biased agonism. a, Left, ExP5–GLP-1R–Gs structure after refinement in the cryo-EM map. Middle, cryo-EM density map coloured by local resolution (Å). Right, low-resolution cryo-EM map highlighting the predominant $G\alpha_s$ α-helical domain location in ExP5–GLP-1R–Gs (grey), compared to β2-AR–Gs (PDB:3SN6, orange). **b**, Transmembrane domain and peptide superimposition reveal backbone differences in ECL3, TM6, TM7 and TM1 when bound by GLP-1 relative to ExP5. ExP5 is located closer to TM1 than GLP-1. **c**, D372 and E373 in ECL3 are important for the pharmacology of GLP-1 and have a limited role in ExP5 affinity and signalling. WT, wild type; V, vehicle. **d**, Left, overlay of the GLP-1–GLP-1R deposited structure[2] (GLP-1R in red) and ExP5–GLP-1R (GLP-1R in blue) reveals a rotation in TM1 side chains. Right, $L141^{1.36}$, $Y145^{1.40}$ and $Y148^{1.43}$ mutations have a larger effect on ExP5-mediated than on GLP-1-mediated cAMP signalling. Whole-cell binding assays and cAMP signalling were assessed in CHOFlpIn cells and data are means + s.e.m. of four (for TM1) and six (for ECL3) independent experiments, performed in duplicate.

bundle that contribute to the positioning of the N termini of GLP-1 and ExP5 (Extended Data Fig. 4b). Notably, the 11-mer agonist-bound GLP-1R structure solved without the $G\alpha_s$ heterotrimer[15] displayed a unique NTD conformation relative to GLP-1 and ExP5 (Extended Data Fig. 4c). Collectively, these structures suggest that the binding of different peptide agonists alters the juxtaposition of the extracellular NTD and transmembrane bundle to regulate the ability of different peptides to activate class B GPCRs.

Compared to inactive class B GPCR transmembrane bundles, the GLP-1R in our structure undergoes similar macroscopic conformational transitions to those previously reported for the GLP-1-bound GLP-1R[2] and calcitonin-bound CTR[9] (Extended Data Fig. 4d–h). These include considerable movements in the extracellular ends of transmembrane (TM) helices 1, 6 and 7, required to open the bundle to accommodate peptide binding, and a large 15–16 Å movement of TM6 away from the central transmembrane domain axis that opens up the cytoplasmic face to accommodate G protein interaction (Extended Data Fig. 4d, f). These large conformational movements are coordinated around the highly conserved class B GPCR $P^{6.47}XXG^{6.50}$ motif in TM6, and $G^{7.50}$ in TM7 (Extended Data Fig. 4d). Nonetheless, there are notable differences in the extracellular face between the activated structures, particularly in the extent of movement of TM6, ECL3 and TM7, which probably reflect the distinct modes with which these ligands activate their respective receptors (Extended Data Fig. 4g, h).

ExP5 is a biased agonist relative to exendin-4[6]. Our pharmacological analysis revealed that ExP5 is also G protein-biased, with limited β-arrestin recruitment relative to GLP-1 (Extended Data Fig. 1d). Comparison of receptor occupancy with ligand potency and efficacy in cellular signalling assays showed that the bias of ExP5 arises primarily from enhanced efficacy in $G\alpha_s$-mediated cAMP signalling, rather than a loss of β-arrestin coupling (Extended Data Fig. 1e). Ligand binding and GTPγS studies performed in insect cells also support enhanced G protein efficacy of ExP5 relative to GLP-1 (Extended Data Fig. 1c). Thus, comparison of the GLP-1 and ExP5-bound GLP-1R–$G\alpha s\beta\gamma$ structures provides insight into conformational differences that may be linked to biased agonism.

The largest distinctions between the GLP-1 and ExP5-bound GLP-1R transmembrane domains occur within TM1, the extracellular portions of TM6 and TM7, and the ECL3 conformation (Fig. 1b, Extended Data Fig. 5a), indicating that these domains may contribute to biased agonism. This is supported by earlier work identifying crucial roles for ECL3, and the extracellular helical boundaries of TM6 and TM7, within the GLP-1R for differential control of GLP-1R-mediated signalling[17]. Alanine scanning mutagenesis confirmed the importance of this domain for the differing pharmacological profiles of GLP-1 and ExP5 (Fig. 1c, Extended Data Table 1). Although some ECL3 residues (G377, R380) had similar roles in both GLP-1 and ExP5 function, the substitutions L379A, D372A and E373A substantially reduced GLP-1 affinity and signalling but had little effect on ExP5 function. Notably, the latter two residues lie within the region of ECL3 where the largest receptor backbone differences are observed between the two structures (Extended Data Fig. 5a), and alanine mutation converts the binding profile of GLP-1 to one that closely resembles the binding profile of ExP5 (Fig. 1c). Mutagenesis of these two residues also had a similar effect on the pharmacology of exendin-4, which has a bias profile similar to that of GLP-1 for these pathways (Extended Data Table 1). Moreover, mutation of $L388^{7.43}$ within the top of TM7 had a greater effect on GLP-1 signalling than on ExP5 signalling (Extended Data Fig. 5b), further supporting the importance of this region in biased agonism of GLP-1R.

There are additional differences between the ExP5-bound structure and the deposited GLP-1-bound GLP-1R structure, in the reported positioning of the TM1 kink and orientation of side chains in the extracellular half of TM1 (Extended Data Fig. 5c, Fig. 1d). The location of the TM1 kink in the 11-mer-bound GLP-1R and the agonist-bound CTR structures is equivalent to that observed in the ExP5-bound structure and an overlay of the ExP5-bound and GLP-1-bound GLP-1R cryo-EM maps reveals that they have similar backbone densities (Extended Data Fig. 5c). Although the limited density in the GLP-1 bound structure precludes confidence, the TM1 backbone can also be modelled in this common conformation, suggesting that the gross positioning of TM1 may be conserved, although comparison of the density maps indicates that the side chain positioning differs between the ExP5- and GLP-1-bound structures, possibly contributing to the biased agonism of ExP5. Indeed, in the deposited GLP-1-bound model, $L141^{1.36}$, $Y145^{1.40}$ and $Y148^{1.43}$ face towards TM7, whereas in the ExP5 structure they reside closer to TM2 (Fig. 1d). Mutation of these residues to alanine had a stronger effect on ExP5-mediated cAMP signalling than on GLP-1 signalling, supporting a role for TM1 in the control of signalling and an interaction between TM1 and TM7–ECL3–TM6 that manifests as altered $G\alpha_s$ efficacy and biased agonism between GLP-1 and ExP5.

Strong density was observed for the entirety of ExP5 extending from the NTD into deep within the transmembrane core (Extended Data Fig. 3).

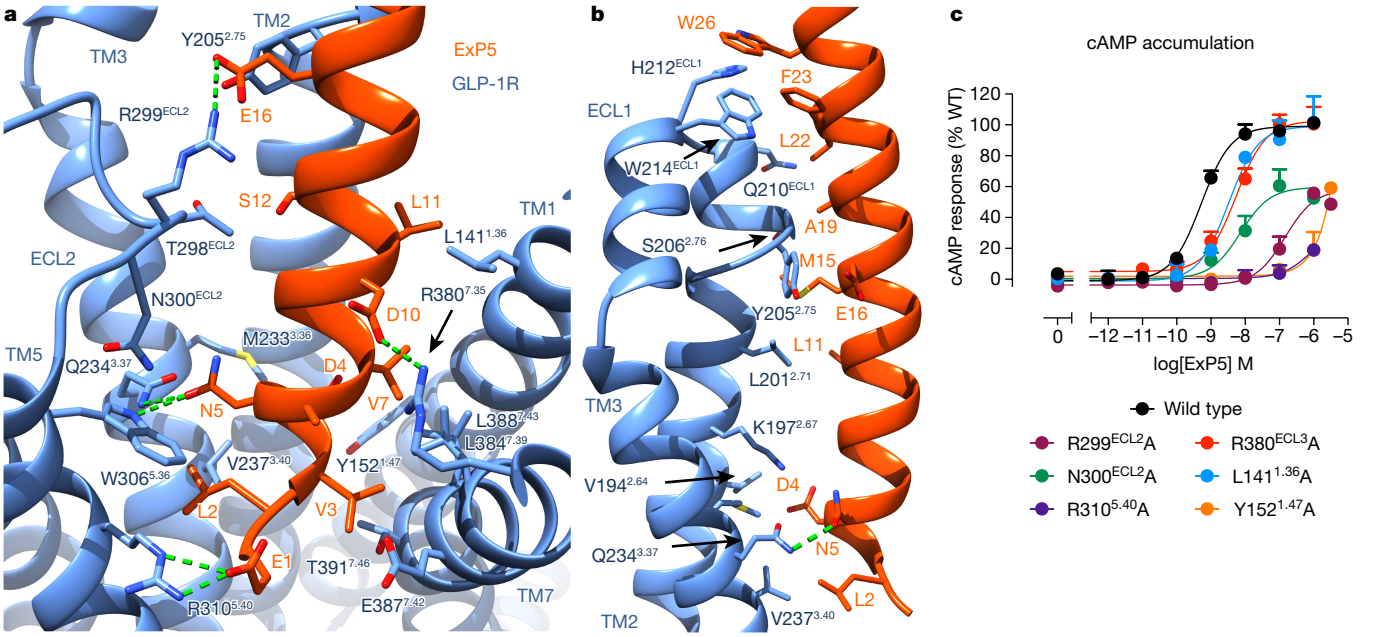

Figure 2 | The ExP5 binding site. a, Key interactions between ExP5 residues and TM1, TM3, TM5, TM7 and ECL2 of the GLP-1R transmembrane bundle (side chains located within 4 Å between the peptide (orange) and the GLP-1R (blue) are shown). ECL3 has been removed for clarity. **b**, Additional interactions formed by ExP5 with TM2, TM3 and ECL1. **c**, The functional effect on Gs-mediated cAMP accumulation following mutagenesis of key ExP5 residues that form interactions (highlighted in **a**) in the refined model supports the role of these residues in ExP5 interactions. cAMP signalling was assessed in CHOFlpIn cells and data are means + s.e.m. of four independent experiments performed in duplicate.

The peptide forms extensive interactions with residues in TMs 1, 2, 3, 5, 7 and all 3 ECLs (Fig. 2, Extended Data Table 2). Alanine mutagenesis confirmed the importance of key residues in the GLP-1R for ExP5 binding (Fig. 2c). Many of these residues lining the ExP5 binding site have previously been implicated as being important for binding of the cognate ligand, GLP-1[7,17–23].

E1 of ExP5 interacts with R310$^{5.40}$ of GLP-1R and is crucial for the ability of ExP5 to promote signalling through Gα_s, with R310$^{5.40}$A almost completely abolishing ExP5-mediated cAMP accumulation (Fig. 2a, c). Very clear density is evident for W306$^{5.36}$, which interacts directly with ExP5 through Van der Waal interactions with the aliphatic region of N5, as well as forming a direct hydrogen bond with N5 in the peptide. N5 also forms a hydrogen bond with Q234$^{3.37}$. N300^{ECL2} points down towards the receptor core within bonding distance of W306$^{5.36}$ and may participate in stabilizing these interactions. A series of contacts occur between residues in TM2 and ExP5, mainly through hydrophobic Van der Waals interactions with either hydrophobic residues or aliphatic regions of polar side chains (Fig. 2b, Extended Data Table 2). Peptide interactions also occur within ECL1, a region that has been implicated in peptide binding of other GLP-1R agonists[17,22] and ECL1 resides close to GLP-1 in the GLP-1-bound cryo-EM structure[2]. Van der Waals interactions are also formed between ExP5 and residues in TM1 and TM7 (Fig. 2a, Extended Data Table 2). In addition, two key electrostatic interactions are formed by R299^{ECL2} in ECL2 and R380$^{7.35}$ at the top of the TM7–ECL3 boundary with E16 and D10 of ExP5, respectively (Fig. 2a). These two residues also formed direct interactions with the 11-mer peptide agonist in the GLP-1R X-ray structure, interacting with a serine at position 8 (R299^{ECL2}) and an aspartic acid at position 9 (R380$^{7.35}$)[15]. D9 in the 11-mer is the equivalent of D10 in ExP5 and D15 in native GLP-1. An interaction between GLP-1 D15 and R380$^{7.35}$ has also been predicted by molecular dynamics simulations[17] and mutagenesis[23], but was not reported in the GLP-1-bound GLP-1R structure[2]. However, side chain densities were poorly resolved in this region of the deposited GLP-1–GLP-1R map; alternative modelling can preserve this interaction and therefore it is likely to be conserved across the three ligands for which structures are now available.

The GLP-1-bound GLP-1R cryo-EM structure also reported that R299^{ECL2} dips into the receptor core to form a direct interaction with H7 of GLP-1[2]. This modelling into the cryo-EM map is also ambiguous and contains an alternate positioning of W306$^{5.36}$ (required for R299^{ECL} to reach into the bundle) to the ExP5-bound and 11-mer-bound GLP-1R structures[15]. Because this positioning of W306$^{5.36}$ is not supported by density, and the described interaction of R299^{ECL2} is highly energetically unfavourable, we hypothesize that W306$^{5.36}$ is more likely to reside in a similar orientation to that observed in the ExP5- and 11-mer-bound structures, supported by good density in these maps. This orientation would promote interactions of R299^{ECL2} with GLP-1 higher up in the peptide.

Owing to the limited density available to define GLP-1 interactions in the GLP-1-bound GLP-1R cryo-EM map, it is difficult to assess direct differences in peptide interactions between the GLP-1- and ExP5-bound structures by relying on the structures alone. Nonetheless, alanine mutation of residues lining the ExP5-binding pocket (highlighted in Fig. 2c, Extended Data Table 1) confirmed a likely overlap of GLP-1R residues involved in interactions with GLP-1 and ExP5, with previous publications highlighting the importance of Y205$^{2.75}$, R299^{ECL2}, N300 ^{ECL2}, R380$^{7.35}$ and R310$^{5.40}$ in GLP-1 affinity and signalling[1,17,20,21], and our results confirming their importance for ExP5 binding (Fig. 2). The nature of these interactions is likely to differ, owing to the variations in peptide sequence and consequent receptor interactions, as highlighted by the TM1, TM7 and ECL3 mutagenesis in this study.

Class B GPCRs contain a number of highly conserved transmembrane polar residues that participate in key hydrogen bond interactions for receptor integrity and maintenance of the apo state. A central polar network formed by residues R$^{2.60}$, N$^{3.43}$, H$^{6.52}$ and Q$^{7.49}$ is located just below the peptide binding site in the ExP5-bound structure[24,25] (Extended Data Fig. 6). Two highly conserved class B GPCR polar networks (TM2–TM3–TM6–TM7: H$^{2.50}$, E$^{3.50}$, T$^{6.42}$, Y$^{7.57}$ and TM2–TM6–TM7–H8: R$^{2.46}$, R/K$^{6.37}$, N$^{7.61}$, E$^{8.41}$) at the cytoplasmic face lock the base of the receptor in an inactive conformation[21,25]. Located between the central hydrogen bond network and the TM2–TM3–TM6–TM7 network is a cluster of conserved residues that form

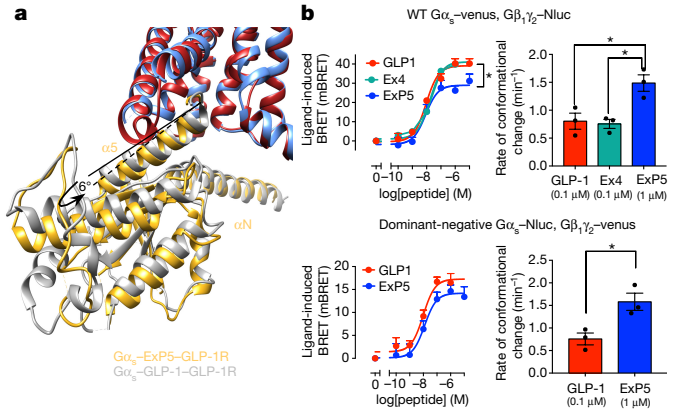

Figure 3 | Comparison of GLP-1R-mediated G protein conformation in GLP-1-bound and ExP5-bound receptors. a, Superimposition of the GLP-1R bundle bound by GLP-1 and by ExP5 reveals distinct angles of $G\alpha_s$ α5 engagement (6° measured using pisco). **b**, Top, BRET measurements show distinct conformational rearrangements between the $G\alpha_s$ α-helical domain and Gγ when the GLP-1R is activated by ExP5, relative to activation by GLP-1 or exendin-4. This is associated with a faster rate of rearrangement at equi-occupant ligand concentrations. Bottom, similar differences are observed with the dominant-negative $G\alpha_s$. Data are means + s.e.m. (left panels) or mean ± s.e.m. (right panels) of three independent experiments performed in triplicate. * $P < 0.05$ by one-way analysis of variance followed by Tukey's multiple comparisons post-test.

hydrophobic packing interactions in the inactive state, stabilizing the TM6 $P^{6.47}XXG^{6.50}$ motif in an inactive conformation (Extended Data Fig. 6). Upon peptide binding, a reorganization of the GLP-1R central hydrogen bond network is associated with destabilization within TM6 around the $P^{6.47}XXG^{6.50}$ motif and a major rearrangement of the central hydrophobic network to form a new packing arrangement that stabilizes the active state (Extended Data Fig. 6, Supplementary Video 1). These major rearrangements break two hydrogen bond networks at the bottom of the receptor, facilitating movement of TM6 away from the transmembrane bundle to create a cavity for G protein binding (Extended Data Figs 6, 7b–d, Supplementary Video 1). $Y^{7.57}$ and $H^{2.50}$ are released from their ground state constraints and reorganize to form part of the hydrophobic network that stabilizes the active state. $E^{3.50}$ maintains a hydrogen bond interaction with $H^{2.50}$, further stabilizing this active conformation.

The GLP-1R active conformation is stabilized by extensive interactions with the $G\alpha_s$ heterotrimeric protein (Extended Data Fig. 7). The receptor–$G\alpha_s$ heterotrimer interface is formed by residues located in TM2, TM3, TM5, TM6, TM7, ICL1, ICL2, ICL3 and H8 of the GLP-1R, and the α5 and αN regions of $G\alpha_s$ and Gβ (Extended Data Table 3).

H8 in all active structures is amphipathic, with bulky aromatic residues on the membrane-proximal face heavily buried in the detergent micelle. Direct interactions of H8 and ICL1 with Gβ are conserved across class B GPCR G protein structures[2,9] (Extended Data Fig. 7e) and these are summarized in Extended Data Table 3. Though the importance of these interactions for the GLP-1R is unclear, truncation of H8 in the CTR reduced receptor expression and peptide-mediated cAMP efficacy, suggesting that receptor–Gβ interactions are important for class B GPCR function[9].

In all structures, the most extensive G protein contacts are formed by the α5 helix of the $G\alpha_s$ Ras-like domain, which inserts into the central GLP-1R transmembrane bundle cytoplasmic cavity formed by the 15 Å outward movement of TM6 (Extended Data Fig. 7). These contacts consist of both polar and hydrophobic Van der Waals interactions and there is, generally, a common interaction pattern between $G\alpha_s$ and the available active class B GPCRs (Extended Data Table 3).

Superimposition of the G proteins of the GLP-1- and ExP5-bound GLP-1R structures reveals only relatively small differences in the receptor-complexed $G\alpha_s$Ras and Gβγ domains (Extended Data Fig. 7f). The largest change was a 4 Å variance in the conformation of the $G\alpha_s\alpha N$ domain at its N terminus, which may reflect a ligand-dependent difference in conformation.

Superimposition of the transmembrane domains of the GLP-1R in the GLP-1- and ExP5- bound structures reveals that, although there are limited differences in the overall $G\alpha_s$Ras and Gβγ conformations, there is a six-degree variance in the angle at which the $G\alpha_s$ α5 helix engages in the GLP-1R cytoplasmic cavity. This results in an overall rotation of the G protein in the ExP5-bound structure relative to the GLP-1-bound structure (Fig. 3a, Extended Data Fig. 7f). Notably, when ExP5 is bound to the GLP-1R, the α4 helix and β3 strand are located further from the receptor core, and no interactions are observed between the α4 helix and the GLP-1R intracellular face, whereas there are potential contacts for the GLP-1-bound structure[2]. In addition, the αN–β3 loop of Gαs is located further from ICL2 of the GLP-1R in the ExP5-bound structure; although these side chains are still within bonding distance, their interactions are likely to be weaker than those induced by GLP-1 binding. Notably, there was only very limited density within the backbone for residues in the bottom of TM5–ICL3 (residues 337–343) in the ExP5-bound structure, such that this region is not visible in high-resolution maps, whereas this backbone density was clearly visible for the GLP-1-bound structure (Extended Data Fig. 5d). This suggests that ICL3 of the GLP-1R is less flexible in the GLP-1- and G protein-bound state than in the ExP5- and G protein-bound state.

There are multiple lines of evidence that differences in ligand–receptor conformation propagate to G protein conformation[26,27]. Direct assessment of conformational rearrangement between $G\alpha_s$ and Gγ, using a bioluminescence resonance energy transfer (BRET) assay, revealed that ExP5 promotes a faster conformational change within $G\alpha_s$ than do GLP-1 or exendin-4 at equi-occupant concentrations, accompanied by a lower BRET maximal signal (E_{max}) at saturating concentrations of peptide (Fig. 3b). Together with the structural data, these results are consistent with the distinct flexibilities of the bottom of TM5 and within ICL3 altering the conformational positioning of the $G\alpha_s$ α-helical domain and increasing the rate of G protein activation. Collectively, this may contribute to the enhanced $G\alpha_s$ protein-mediated efficacy of ExP5 that is a key element of its biased agonism.

In conclusion, the structure of the ExP5–GLP-1R–$G\alpha_s$ complex provides insights into the structural reorganization of class B GPCRs upon peptide activation, as well as the distinct engagement of GLP-1R agonists with differential signalling bias. Our results highlight that even when ligands share a common G protein transducer, differences in the mode of G protein binding can have consequences for conformational changes in the G protein that are linked to activation. The findings increase our understanding of biased agonism and may contribute to the rational design of novel therapeutics that target the GLP-1R.

Online Content Methods, along with any additional Extended Data display items and Source Data, are available in the online version of the paper; references unique to these sections appear only in the online paper.

Received 22 September 2017; accepted 17 January 2018.
Published online 21 February 2018.

1. de Graaf, C. *et al.* Glucagon-like peptide-1 and its class B G protein-coupled receptors: a long march to therapeutic successes. *Pharmacol. Rev.* **68,** 954–1013 (2016).
2. Zhang, Y. *et al.* Cryo-EM structure of the activated GLP-1 receptor in complex with a G protein. *Nature* **546,** 248–253 (2017).
3. Hager, M. V., Clydesdale, L., Gellman, S. H., Sexton, P. M. & Wootten, D. Characterization of signal bias at the GLP-1 receptor induced by backbone modification of GLP-1. *Biochem. Pharmacol.* **136,** 99–108 (2017).
4. Koole, C. *et al.* Allosteric ligands of the glucagon-like peptide 1 receptor (GLP-1R) differentially modulate endogenous and exogenous peptide responses in a pathway-selective manner: implications for drug screening. *Mol. Pharmacol.* **78,** 456–465 (2010).
5. Wootten, D. *et al.* Differential activation and modulation of the glucagon-like peptide-1 receptor by small molecule ligands. *Mol. Pharmacol.* **83,** 822–834 (2013).
6. Zhang, H. *et al.* Autocrine selection of a GLP-1R G-protein biased agonist with potent antidiabetic effects. *Nat. Commun.* **6,** 8918 (2015).

7. Mann, R. *et al.* Peptide binding at the GLP-1 receptor. *Biochem. Soc. Trans.* **35,** 713–716 (2007).
8. Manandhar, B. & Ahn, J. M. Glucagon-like peptide-1 (GLP-1) analogs: recent advances, new possibilities, and therapeutic implications. *J. Med. Chem.* **58,** 1020–1037 (2015).
9. Liang, Y. L. *et al.* Phase-plate cryo-EM structure of a class B GPCR–G-protein complex. *Nature* **546,** 118–123 (2017).
10. Danev, R., Buijsse, B., Khoshouei, M., Plitzko, J. M. & Baumeister, W. Volta potential phase plate for in-focus phase contrast transmission electron microscopy. *Proc. Natl Acad. Sci. USA* **111,** 15635–15640 (2014).
11. Khoshouei, M., Radjainia, M., Baumeister, W. & Danev, R. Cryo-EM structure of haemoglobin at 3.2 Å determined with the Volta phase plate. *Nat. Commun.* **8,** 16099 (2017).
12. Khoshouei, M. *et al.* Volta phase plate cryo-EM of the small protein complex Prx3. *Nat. Commun.* **7,** 10534 (2016).
13. Siu, F. Y. *et al.* Structure of the human glucagon class B G-protein-coupled receptor. *Nature* **499,** 444–449 (2013).
14. Hollenstein, K. *et al.* Structure of class B GPCR corticotropin-releasing factor receptor 1. *Nature* **499,** 438–443 (2013).
15. Jazayeri, A. *et al.* Crystal structure of the GLP-1 receptor bound to a peptide agonist. *Nature* **546,** 254–258 (2017).
16. Runge, S., Thøgersen, H., Madsen, K., Lau, J. & Rudolph, R. Crystal structure of the ligand-bound glucagon-like peptide-1 receptor extracellular domain. *J. Biol. Chem.* **283,** 11340–11347 (2008).
17. Wootten, D. *et al.* The extracellular surface of the GLP-1 receptor is a molecular trigger for biased agonism. *Cell* **165,** 1632–1643 (2016).
18. Coopman, K. *et al.* Residues within the transmembrane domain of the glucagon-like peptide-1 receptor involved in ligand binding and receptor activation: modelling the ligand-bound receptor. *Mol. Endocrinol.* **25,** 1804–1818 (2011).
19. Dods, R. L. & Donnelly, D. The peptide agonist-binding site of the glucagon-like peptide-1 (GLP-1) receptor based on site-directed mutagenesis and knowledge-based modelling. *Biosci. Rep.* **36,** e00285 (2015).
20. Koole, C. *et al.* Second extracellular loop of human glucagon-like peptide-1 receptor (GLP-1R) has a critical role in GLP-1 peptide binding and receptor activation. *J. Biol. Chem.* **287,** 3642–3658 (2012).
21. Wootten, D. *et al.* Key interactions by conserved polar amino acids located at the transmembrane helical boundaries in class B GPCRs modulate activation, effector specificity and biased signalling in the glucagon-like peptide-1 receptor. *Biochem. Pharmacol.* **118,** 68–87 (2016).
22. Yang, D. *et al.* Structural determinants of binding the seven-transmembrane domain of the glucagon-like peptide-1 receptor (GLP-1R). *J. Biol. Chem.* **291,** 12991–13004 (2016).
23. Moon, M. J. *et al.* Ligand binding pocket formed by evolutionarily conserved residues in the glucagon-like peptide-1 (GLP-1) receptor core domain. *J. Biol. Chem.* **290,** 5696–5706 (2015).
24. Wootten, D. *et al.* A hydrogen-bonded polar network in the core of the glucagon-like peptide-1 receptor is a fulcrum for biased agonism: lessons from class B crystal structures. *Mol. Pharmacol.* **89,** 335–347 (2016).
25. Wootten, D., Simms, J., Miller, L. J., Christopoulos, A. & Sexton, P. M. Polar transmembrane interactions drive formation of ligand-specific and signal pathway-biased family B G protein-coupled receptor conformations. *Proc. Natl Acad. Sci. USA* **110,** 5211–5216 (2013).
26. Furness, S. G. B. *et al.* Ligand-dependent modulation of G protein conformation alters drug efficacy. *Cell* **167,** 739–749.e11 (2016).
27. Gregorio, G. G. *et al.* Single-molecule analysis of ligand efficacy in β2AR-G-protein activation. *Nature* **547,** 68–73 (2017).

Supplementary Information is available in the online version of the paper.

Acknowledgements The work was supported by the Monash University Ramaciotti Centre for Cryo-Electron Microscopy, the National Health and Medical Research Council of Australia (NHMRC) project grants (1061044, 1065410, 1120919 and 1126857), NHMRC program grant (1055134), Strategic Priority Research Program of the Chinese Academy of Sciences (XDA12020347) and Shanghai Science and Technology Development Fund (15DZ2291600). P.M.S., A.C., D.W. and C.K. are NHMRC Principal Research, Senior Principal Research, Career Development and CJ Martin Fellows, respectively. S.L. received the Postgraduate Overseas Study Fellowship from CAS. We thank J. Plitzko, G. Christopoulos, V. Julita, J. Michaelis, X. Zhang, P. Thompson and M. Liu for assay and technical support and B. Kobilka for technical advice and comments on the manuscript.

Author Contributions Y.-L.L. established the GLP-1R complex expression and purification strategy, expressed and purified the complex, and performed negative stain EM and data acquisition/analysis; Y.-L.L. and M.R. performed preliminary cryo-EM screening; M.K. performed cryo-sample preparation and phase plate imaging to acquire EM data and performed EM map calculations; A.G. built the model and performed refinement; A.G., C.K. and D.M.T. performed pharmacological assays; L.C., T.T.T. and S.L. performed the mutagenesis studies; S.G.B.F. and P.Z. designed and performed the G protein BRET assays; R.D. and W.B. organized and developed the Volta phase plate cryo-EM data acquisition strategy; Y.-L.L., M.K., A.G., S.G.B.F., P.Z., L.C., C.K., D.M.T., T.T.T., S.L., A.C., P.M.S. and D.W. performed data analysis; S.G.B.F., P.Z., C.K., A.C., L.J.M., M.-W.W. and A.C. assisted with data interpretation and preparation of the manuscript; Y.L.L., M.K., A.G., P.M.S. and D.W. interpreted data and wrote the manuscript; P.M.S. and D.W. supervised the project.

Author Information Reprints and permissions information is available at www.nature.com/reprints. The authors declare no competing financial interests. Readers are welcome to comment on the online version of the paper. Publisher's note: Springer Nature remains neutral with regard to jurisdictional claims in published maps and institutional affiliations. Correspondence and requests for materials should be addressed to D.W. (denise.wootten@monash.edu) and P.M.S. (Patrick.sexton@monash.edu).

Reviewer Information *Nature* thanks R. Glaeser, F. Marshall and J. Mayer for their contribution to the peer review of this work.

METHODS

Constructs. The human GLP-1R was unmodified with the exception of replacing the native signal peptide with that of haemagglutinin (HA) to enhance receptor expression and the addition of affinity tags (an N-terminal Flag tag epitope and a C-terminal 8× His tag); both tags are removable by 3C protease cleavage. The construct was generated in both mammalian and insect cell expression vectors. These modifications did not alter receptor pharmacology (Extended Data Fig. 1b). A dominant-negative $G\alpha_s$ ($DNG\alpha_s$) construct was generated by site-directed mutagenesis to incorporate mutations that alter nucleotide handling (S54N[28] and G226A[29]), stabilize the G_0 state (E268A[30]) and substitute residues from $G\alpha_{i2}$ (N271K, K274D, R280K, T284D and I285T[31,32]) that are reported to improve the dominant-negative effect, presumably by stabilizing interactions with the $\beta\gamma$ subunits.

Insect cell expression. Human GLP-1R, human $DNG\alpha_s$, and His_6-tagged human $G\beta_1$ and $G\gamma_2$ were expressed in Tni insect cells (Expression systems) using baculovirus. Cell cultures were grown in ESF 921 serum-free medium (Expression Systems) to a density of 4 million cells per ml and then infected with three separate baculoviruses at a ratio of 2:2:1 for GLP-1R, $DNG\alpha_s$ and $G\beta_1\gamma_2$. The culture was collected by centrifugation 60 h after infection and cell pellets were stored at −80 °C.

Complex purification. Cell pellets were thawed in 20 mM HEPES pH 7.4, 50 mM NaCl, 2 mM $MgCl_2$ supplemented with cOmplete Protease Inhibitor Cocktail tablets (Roche). Complex formation was initiated by addition of 1 μM ExP5 (China Peptides), Nb35–His (10 μg/ml) and apyrase (25 mU/ml, NEB); the suspension was incubated for 1 h at room temperature. Membranes were collected by centrifugation at 30,000*g* for 30 min, and complex was solubilized from membrane using 0.5% (w/v) lauryl maltose neopentyl glycol (LMNG, Anatrace) supplemented with 0.03% (w/v) cholesteryl hemisuccinate (CHS, Anatrace) for 2 h at 4 °C in the presence of 1 μM ExP5 and apyrase (25 mU/ml, NEB). Insoluble material was removed by centrifugation at 30,000*g* for 30 min and the solubilized complex was immobilized by batch binding to M1 anti-Flag affinity resin in the presence of 3 mM $CaCl_2$. The resin was packed into a glass column and washed with 20 column volumes of 20 mM HEPES pH 7.4, 100 mM NaCl, 2 mM $MgCl_2$, 3 mM $CaCl_2$, 1 μM ExP5, 0.01% (w/v) LMNG and 0.006% (w/v) CHS before bound material was eluted in buffer containing 5 mM EGTA and 0.1 mg/ml FLAG peptide. The complex was then concentrated using an Amicon Ultra Centrifugal Filter (MWCO, 100 kDa) and subjected to size-exclusion chromatography on a Superdex 200 Increase 10/300 column (GE Healthcare) that was pre-equilibrated with 20 mM HEPES pH 7.4, 100 mM NaCl, 2 mM $MgCl_2$, 1 μM ExP5, 0.01% (w/v) MNG and 0.006% (w/v) CHS to separate complex from contaminants. Eluted fractions consisting of receptor and G-protein complex were pooled and concentrated. The final yield of purified complex was approximately 0.2 mg per litre of insect cell culture.

SDS–PAGE and western blot analysis. Samples collected from size-exclusion chromatography were analysed by SDS–PAGE and western blot. For SDS–PAGE, precast gradient TGX gels (Bio-Rad) were used. Gels were either stained by Instant Blue (Expedeon) or immediately transferred to PVDF membrane (Bio-Rad) at 100 V for 1 h. The proteins on the PVDF membrane were probed with two primary antibodies, rabbit anti-$G\alpha_s$ C-18 antibody (cat. no. sc-383, Santa Cruz) against the $G\alpha_s$ subunit and mouse penta-His antibody (cat. no. 34660, QIAGEN) against His tags. The membrane was washed and incubated with secondary antibodies (680RD goat anti-mouse and 800CW goat anti-rabbit, LI-COR). Bands were imaged using an infrared imaging system (LI-COR Odyssey Imaging System).

Preparation of vitrified specimen. EM grids (Quantifoil, 200 mesh copper R1.2/1.3) were glow discharged for 30 s in high pressure air using Harrick plasma cleaner. Four microlitres of sample at 1.3 mg/ml was applied to the grid in the Vitrobot chamber (FEI Vitrobot Mark IV). The Vitrobot chamber was set to 100% humidity at 4 °C. The sample was blotted for 5 s with a blot force of 20 and then plunged into propane–ethane mixture (37% ethane and 63% propane).

Data acquisition. Data were collected on a Titan Krios microscope operated at 300 kV (Thermo Fisher Scientific equipped with a Gatan Quantum energy filter, a Gatan K2 summit direct electron detector (Gatan) and a Volta phase plate (Thermo Fisher Scientific)). Videos were recorded in EFTEM nanoprobe mode, with 50-μm C2 aperture, at a calibrated magnification of 47,170 corresponding to a magnified pixel size of 1.06 Å. Each video comprised 50 frames with a total dose of 50 $e^-/Å^2$ and exposure time was 8 s with a dose rate of 7 e^- per pixel per s on the detector. Data acquisition was done using SerialEM software at −500 nm defocus[33].

Data processing. We collected 2,793 movies and subjected them to motion correction using motioncor2[34]. Contrast transfer function (CTF) estimation was done using Gctf software[35] on the non-dose-weighted micrographs. The particles were picked using gautomatch (developed by K. Zhang, MRC Laboratory of Molecular Biology, Cambridge, UK; http://www.mrc-lmb.cam.ac.uk/kzhang/Gautomatch/). An initial model was made using EMAN2[36] based on a few automatically picked micrographs and using the common-line approach. The particles were extracted in RELION 2.03[37] using a box size of 200 pixels. Picked particles (614,883) were subjected to 3D classification with 5 classes. Particles (190,135) from the best-looking class were subjected to 3D auto-refinement in RELION 2.03. The refined particles were subjected to another run of 3D classification with 5 classes and without alignments, after which 184,672 particles were chosen for a final run of 3D auto-refinement in RELION 2.03. The final map was sharpened with a *B*-factor of −50 Å. Local resolution was determined using RELION[37] with half-reconstructions as input maps. The cryo-EM data collection, refinement and validation statistics are reported in Supplementary Table 1.

Modelling. The initial template for GLP-1R transmembrane regions, G protein and Nb35 was derived from rabbit GLP-1R in complex with $G\alpha_s$ (PDB-5VAI)[2] followed by extensive remodelling using COOT[38]. The ECL3 loop residues 372–376 were stubbed owing to insufficient density for unambiguous modelling, and no high-resolution density was present for ICL3 residues N338–T343, which were omitted from the deposited structure. Owing to discontinuous and/or variable density in the GLP-1R ECD region, we used the high-resolution X-ray crystal structure of the GLP-1R ECD–exendin(9–39) (PDB-3C5T)[16] for a rigid body fit with limited manual adjustments. The ExP5 peptide was modelled manually. The final model was subjected to global refinement and minimization in real space using the module 'phenix.real_space_refine' in PHENIX[39]. Validation was performed in MolProbity[40].

Insect cell membrane preparations. Crude membrane preparations were prepared from insect cells produced using the same expression conditions as used for cryo-EM samples. Cells were resuspended in buffer (20 mM HEPES 7.4, 50 mM NaCl, 2 mM $MgCl_2$, with protease inhibitors and benzonase) and dounced 20 times with the tight pestle, followed by centrifugation (10 min, 350*g*, 4 °C). The pellet was resuspended in buffer, dounced and clarified by centrifugation at a low *g*. Membranes were pelleted by centrifugation (1 h, 40,000*g*, 4 °C), resuspended in buffer and sonicated. Protein concentration was determined using Bradford reagent (Bio-Rad).

[^{35}S]GTPγS binding. Measurement of [^{35}S]GTPγS incorporation was performed in 20 mM HEPES pH 7.4; 100 mM NaCl; 10 mM $MgCl_2$; 1 mM EDTA; 0.1% (w/v) BSA; 30 μg/ml saponin. Membranes (50 μg per sample) were pre-incubated with 1 μM GDP and increasing concentrations of ligand for 30 min at 22 °C. Reactions were started by the addition of [^{35}S]GTPγS and ATP (final concentrations: 300 pM and 50 μM, respectively). After 1 h incubation at 30 °C, the reaction was terminated by collecting the membranes on Whatman UniFilter GF/C plates using Filtermate 196 harvester (Packard). Membranes were extensively washed with ice-cold 50 mM Tris pH 7.6, 10 mM $MgCl_2$, 100 mM NaCl, dried, dissolved in 40 μl MicroScint-O scintillation cocktail (Packard) and counted using a MicroBeta LumiJET counter (PerkinElmer). Data from each experiment were normalized to the response of GLP-1R–WT$G\alpha_s$–$G\beta_1\gamma_2$ membranes at 1 μM GLP-1 (100%).

Radioligand competition binding experiments on insect cell membranes. Radioligand binding was performed in 20 mM HEPES, pH 7.4, 100 mM NaCl, 10 mM $MgCl_2$ and 0.1% (w/v) BSA. Competition binding assays with GLP-1 and ExP5 were performed in the presence of 50 pM [^{125}I]-exendin(9–39). Binding reactions were initiated with the addition of 4 μg of GLP-1R-expressing membranes (with or without G protein) followed by 1 h incubation at 30 °C. Membranes were collected on UniFilter GF/C (Whatman) plates using a Filtermate 196 harvester (Packard), extensively washed with ice-cold NaCl, dried, dissolved in 40 μl of MicroScint-O scintillation cocktail (Packard), and counted using a MicroBeta LumiJET counter (PerkinElmer). Data from each experiment were normalized to vehicle control and non-specific binding (1 μM exendin(9–39)). Curves were fit to a one- or two-site competition binding equation in Prism 6.0 (GraphPad).

Generation of mutant receptor constructs in mammalian cell lines. Mutant receptors were generated in a 2× c-Myc epitope-tagged receptor in the pEF5/FRT/V5-DEST vector using QuikChange site-directed mutagenesis (Invitrogen) and sequences confirmed. Mutant receptors were stably expressed in CHOFlpIn cells using the FlpIn Gateway technology system (Invitrogen) and selected using 600 μg/ml hygromyocin B. All cells were tested and found to be free from mycoplasma contamination.

Mammalian whole-cell radioligand binding assays. Cells were seeded at a density of 30,000 cells per well into 96-well culture plates and incubated overnight in DMEM containing 5% FBS at 37 °C in 5% CO_2. Growth medium was replaced with binding buffer (DMEM containing 25 mM HEPES and 0.1% (w/v) BSA) containing 0.1 nM [^{125}I]-exendin(9–39) and increasing concentrations of unlabelled peptide agonists. Cells were incubated overnight at 4 °C, followed by three washes in ice cold 1× PBS to remove unbound radioligand. Cells were then solubilized in 0.1 M NaOH, and radioactivity determined by gamma counting. For all experiments, nonspecific binding was defined by 1 μM exendin(9–39).

Mammalian cAMP assays. Cells were seeded at a density of 30,000 cells per well into 96-well culture plates and incubated overnight in DMEM containing 5% FBS at 37 °C in 5% CO_2. cAMP detection was performed as previously described[3]. All values were converted to cAMP concentration using a cAMP standard curve

performed in parallel and data were subsequently normalized to the response of 100 μM forskolin in each cell line.

β-Arrestin recruitment assay. Cells stably expressing GLP-1R–Rluc8 and β-arrestin1–venus were seeded at a density of 30,000 cells per well into 96-well culture plates and incubated overnight in DMEM containing 5% FBS at 37 °C in 5% CO_2. β-Arrestin recruitment was performed as previously described[41].

Mammalian cell membrane preparations for G protein BRET assays. HEK293AΔS-GLP-1R cells were transfected with $G\alpha_s$–venus (inserted at position 72 of $G\alpha_s$ with a GSSSSG linker) or dominant-negative $G\alpha_s$–nanoluc (inserted at position 72 of $G\alpha_s$ with a GSSSSG linker), $G\beta_1$ and $G\gamma_{2}$–nanoluc or $G\gamma_{2}$–venus (inserted at the N terminus of $G\gamma_2$ with a GSAGT linker) at a 1:1:1 ratio using PEI. Cell membranes were prepared as described previously[26] and stored at −80 °C. Twenty-four hours after transfection, cells were collected with membrane preparation buffer (20 mM BisTris, pH 7.4, 50 mM NaCl, 1 mM $MgCl_2$, 1× P8340 protease inhibitor cocktail (Sigma-Aldrich), 1 mM DTT and 0.1 mM PMSF). Cells were then homogenized, applied to a stepped sucrose gradient (60%, 40%, homogenate) and centrifuged at 22,500 r.p.m. for 2.5 h at 4 °C. The layers between 40% and homogenate were collected, diluted in membrane preparation buffer and centrifuged at 30,000 r.p.m. for 30 min at 4 °C. The final pellet was resuspended in membrane preparation buffer, and stored at −80 °C. Total protein concentration was determined using a NanoDrop.

G protein conformational determination using BRET. HEK293AΔS cells stably expressing the GLP-1R (tested and confirmed to be free from mycoplasma) were transfected with a 1:1:1 ratio of $G\gamma_2$:nanoluc–$G\alpha_s$[72]:venus–$G\beta_1$ or $G\gamma_2$:venus–dominant-negative $G\alpha_s$[72]:nanoluc–$G\beta_1$ 24 h before collection and preparation of cell plasma membranes (above). Five micrograms per well of cell membrane was incubated with furimazine (1:1,000 dilution from stock) in assay buffer (1× HBSS, 10 mM HEPES, 0.1% (w/v) BSA, 1× P8340 protease inhibitor cocktail, 1 mM DTT and 0.1 mM PMSF, pH 7.4). The GLP-1R-induced BRET signal between $G\alpha_s$ and $G\gamma$ was measured at 30 °C using a PHERAstar (BMG LabTech). Baseline BRET measurements were taken for 2 min before addition of vehicle or ligand. BRET was measured at 15 s intervals for a further 7 min. All assays were performed in a final volume of 100 μl.

Data analysis. Pharmacological data were analysed using Prism 7 (GraphPad). Concentration-dependent response signalling data were analysed as previously described[20] using a three-parameter logistic equation. Signalling bias was quantified by analysis of cAMP accumulation and β-arrestin1 recruitment concentration–response curves using an operational model of agonism modified to directly estimate the ratio of τ/K_A as described previously[5,20,42].

$$Y = \frac{E_{max} \times (\tau_c/K_A)^n \times [A]^n}{[A]^n \times (\tau_c/K_A)^n + (1 + [A]/K_A)^n}$$

in which E_{max} represents the maximal stimulation of the system, K_A is the agonist–receptor dissociation constant in molar concentration, $[A]$ is the molar concentration of ligand and τ is the operational measure of efficacy in the system, which incorporates signalling efficacy and receptor density. All estimated τ/K_A ratios included propagation of error for both τ and K_A. Changes in τ/K_A ratios with respect to GLP-1 for each novel peptide were used to quantify bias between signalling pathways. Accordingly, bias factors included propagation of error from the τ/K_A ratios of each pathway.

Changes in the rate of change in BRET signal were fitted to a one-phase association curve. Normalized AUC for the indicated ligand concentrations was plotted as a concentration–response curve and fitted with a three-parameter logistic curve. Statistical analysis was performed with either one-way analysis of variance and a Tukey's post-test or a paired *t*-test, and significance accepted at $P < 0.05$.

Graphics. Molecular graphics images were produced using the UCSF Chimera package from the Computer Graphics Laboratory, University of California, San Francisco (supported by NIH P41 RR-01081)[43]. Superposition of maps was performed in COOT using "transformation by LSQ model fit"[38]. Measurements of GαRas α5 movements between different structures was performed in Pymol using the psico python module.

Data availability. All relevant data are available from the authors and/or included in the manuscript or Supplementary Information. Atomic coordinates and the cryo-EM density map have been deposited in the Protein Data Bank (PDB) under accession number 6B3J and EMDB entry ID EMD-7039.

28. Cleator, J. H., Mehta, N. D., Kurtz, D. T. & Hildebrandt, J. D. The N54 mutant of Gαs has a conditional dominant negative phenotype which suppresses hormone-stimulated but not basal cAMP levels. *FEBS Lett.* **443,** 205–208 (1999).
29. Lee, E., Taussig, R. & Gilman, A. G. The G226A mutant of Gsα highlights the requirement for dissociation of G protein subunits. *J. Biol. Chem.* **267,** 1212–1218 (1992).
30. Iiri, T., Bell, S. M., Baranski, T. J., Fujita, T. & Bourne, H. R. A Gsα mutant designed to inhibit receptor signaling through Gs. *Proc. Natl Acad. Sci. USA* **96,** 499–504 (1999).
31. Berlot, C. H. A highly effective dominant negative αs construct containing mutations that affect distinct functions inhibits multiple Gs-coupled receptor signaling pathways. *J. Biol. Chem.* **277,** 21080–21085 (2002).
32. Berlot, C. H. & Bourne, H. R. Identification of effector-activating residues of Gsα. *Cell* **68,** 911–922 (1992).
33. Mastronarde, D. N. Automated electron microscope tomography using robust prediction of specimen movements. *J. Struct. Biol.* **152,** 36–51 (2005).
34. Zheng, S. Q. *et al.* MotionCor2: anisotropic correction of beam-induced motion for improved cryo-electron microscopy. *Nat. Methods* **14,** 331–332 (2017).
35. Zhang, K. Gctf: Real-time CTF determination and correction. *J. Struct. Biol.* **193,** 1–12 (2016).
36. Tang, G.*et al.* EMAN2: an extensible image processing suite for electron microscopy. *J. Struct. Biol.* **157,** 38–46 (2007).
37. Kimanius, D., Forsberg, B. O., Scheres, S. H. & Lindahl, E. Accelerated cryo-EM structure determination with parallelisation using GPUs in RELION-2. *eLife* **5,** e18722 (2016).
38. Emsley, P. & Cowtan, K. Coot: model-building tools for molecular graphics. *Acta Crystallogr. D* **60,** 2126–2132 (2004).
39. Adams, P. D. *et al.* PHENIX: a comprehensive Python-based system for macromolecular structure solution. *Acta Crystallogr. D* **66,** 213–221 (2010).
40. Chen, V. B. *et al.* MolProbity: all-atom structure validation for macromolecular crystallography. *Acta Crystallogr. D* **66,** 12–21 (2010).
41. Savage, E. E., Wootten, D., Christopoulos, A., Sexton, P. M. & Furness, S. G. A simple method to generate stable cell lines for the analysis of transient protein–protein interactions. *Biotechniques* **54,** 217–221 (2013).
42. Hager, M. V. J., Johnson, L. M., Wootten, D., Sexton, P. M. & Gellman, S. H. β-Arrestin-biased agonists of the GLP-1 receptor from β-amino acid residue incorporation into GLP-1 analogues. *J. Am. Chem. Soc.* **138,** 14970–14979 (2016).
43. Pettersen, E. F. *et al.* UCSF Chimera—a visualization system for exploratory research and analysis. *J. Comput. Chem.* **25,** 1605–1612 (2004).
44. Ehlert, F. J. The relationship between muscarinic receptor occupancy and adenylate cyclase inhibition in the rabbit myocardium. *Mol. Pharmacol.* **28,** 410–421 (1985).

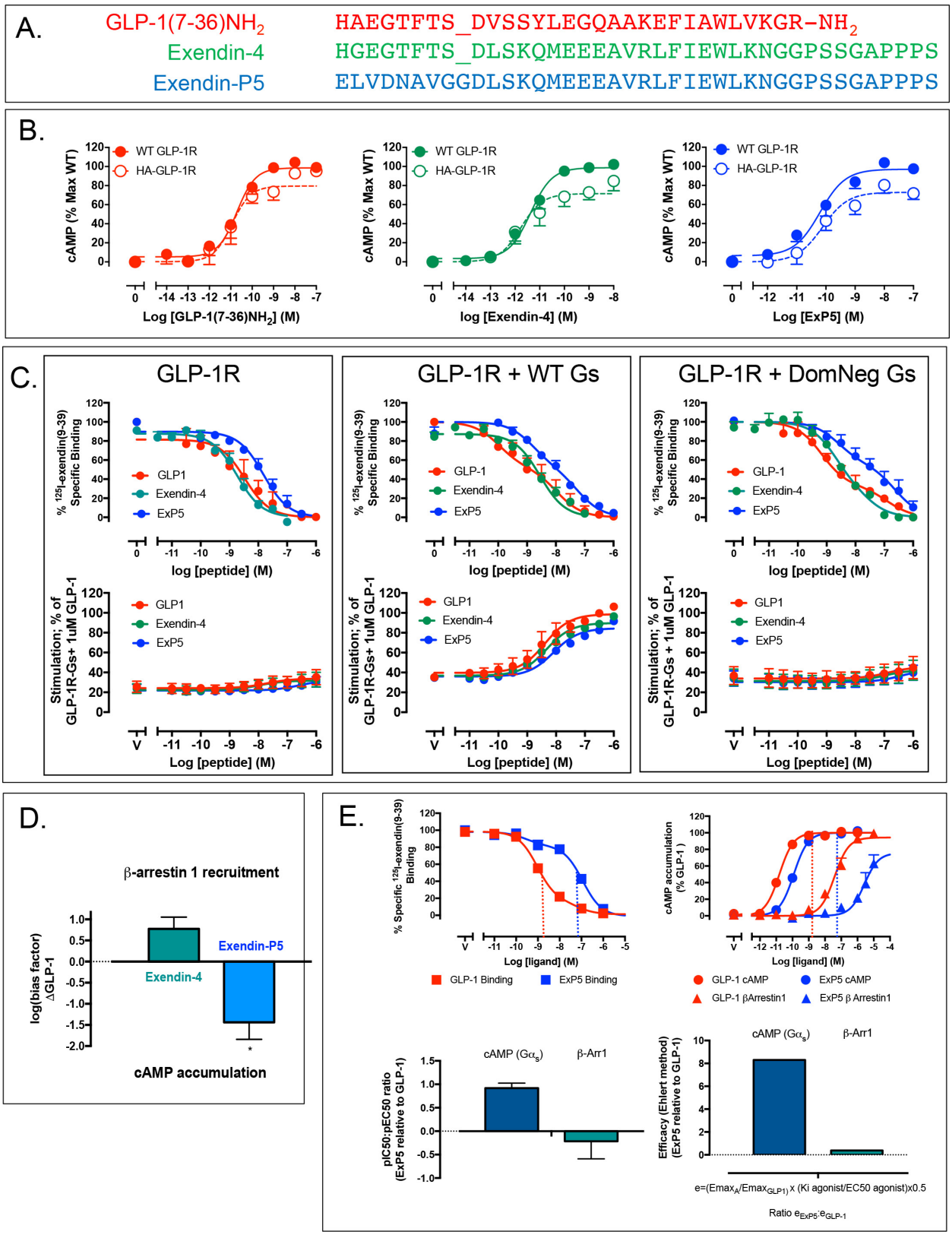

Extended Data Figure 1 | See next page for caption.

Extended Data Figure 1 | GLP-1R pharmacology. a, Peptide sequences. **b**, Pharmacology of untagged GLP-1R (WT GLP-1R) and the purification construct (HA–GLP-1R). **c**, Insect cell pharmacology of HA–GLP-1R. Top, radioligand competition binding. Bottom, GTPγS binding. Left, no Gs protein. ExP5 has lower affinity than GLP-1 and exendin-4 and does not bind GTPγS. Middle, wild-type Gs enhances peptide affinity and promotes GTPγS binding. Right, dominant-negative Gs is similar to wild-type Gs in binding, but does not bind GTPγS. **d**, Bias factors calculated from concentration–response curves using the Black and Leff operational model[5,20,41] (see Methods) confirm that ExP5 is a biased agonist relative to GLP-1. **e**, Top left, pIC_{50} of ExP5 is ~100-fold lower than of GLP-1 (CHOFlpIn whole cell). Top right, GLP-1 and ExP5 have β-arrestin1 coupling with pEC_{50} ~30-fold to the right of their pIC_{50} (dotted lines). ExP5 is more potent than GLP-1 in cAMP signalling (pEC_{50} relative to pIC_{50}). Bottom left, pIC_{50}:pEC_{50} ratios for G protein (cAMP) and β-arrestin1 of ExP5 relative to GLP-1 highlights ExP5 bias arises from enhanced Gs coupling, not reduced β-arrestin1 recruitment. Bottom right, ratio of ExP5 efficacy (calculated using the Ehlert method[44]) relative to GLP-1 in cAMP and β-arrestin1 recruitment confirms that ExP5 bias arises from enhanced $G\alpha_s$ efficacy. Data in **b**, **c** are mean ± s.e.m. of three (insect cells) or four (CHOFlpIn cells) independent experiments, conducted in duplicate or triplicate, respectively. Data in **d**, **e** are from 11 independent experiments performed in duplicate. $^*P < 0.05$ by one-way analysis of variance and Dunnett's post-test.

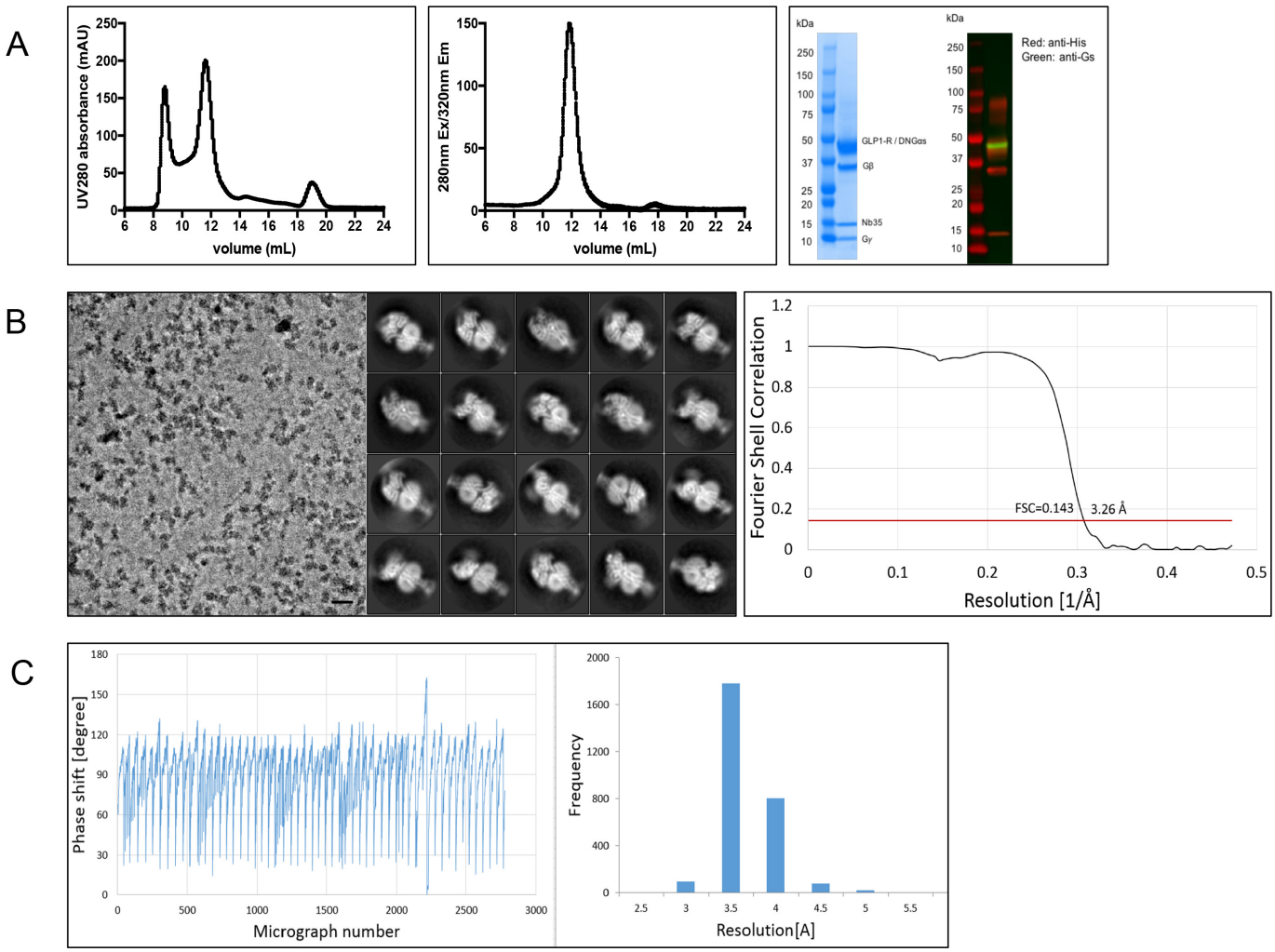

Extended Data Figure 2 | Purification and Volta phase plate imaging of the ExP5–GLP-1R–Gs complex. a, Left, elution profile of the purified complex. Middle, pooled complex fractions, concentrated and analysed by size exclusion chromatography (SEC). Right, SDS–PAGE/Coomassie blue stain and western blot of the complex showing all components. Anti-His antibody detects Flag–GLP-1R–His, Gβ–His and Nb35–His (red) and anti-Gs antibody detects $G\alpha_s$ (green). **b**, Left, Volta phase plate micrograph of the complex (representative of 2,793). Middle, 2D class averages. Right; 'gold standard' Fourier shell correlation (FSC) curves; the overall nominal resolution is 3.26 Å. **c**, Left, Volta phase plate phase shift history throughout the dataset. Right, histogram of the estimated micrograph resolutions from the CTF.

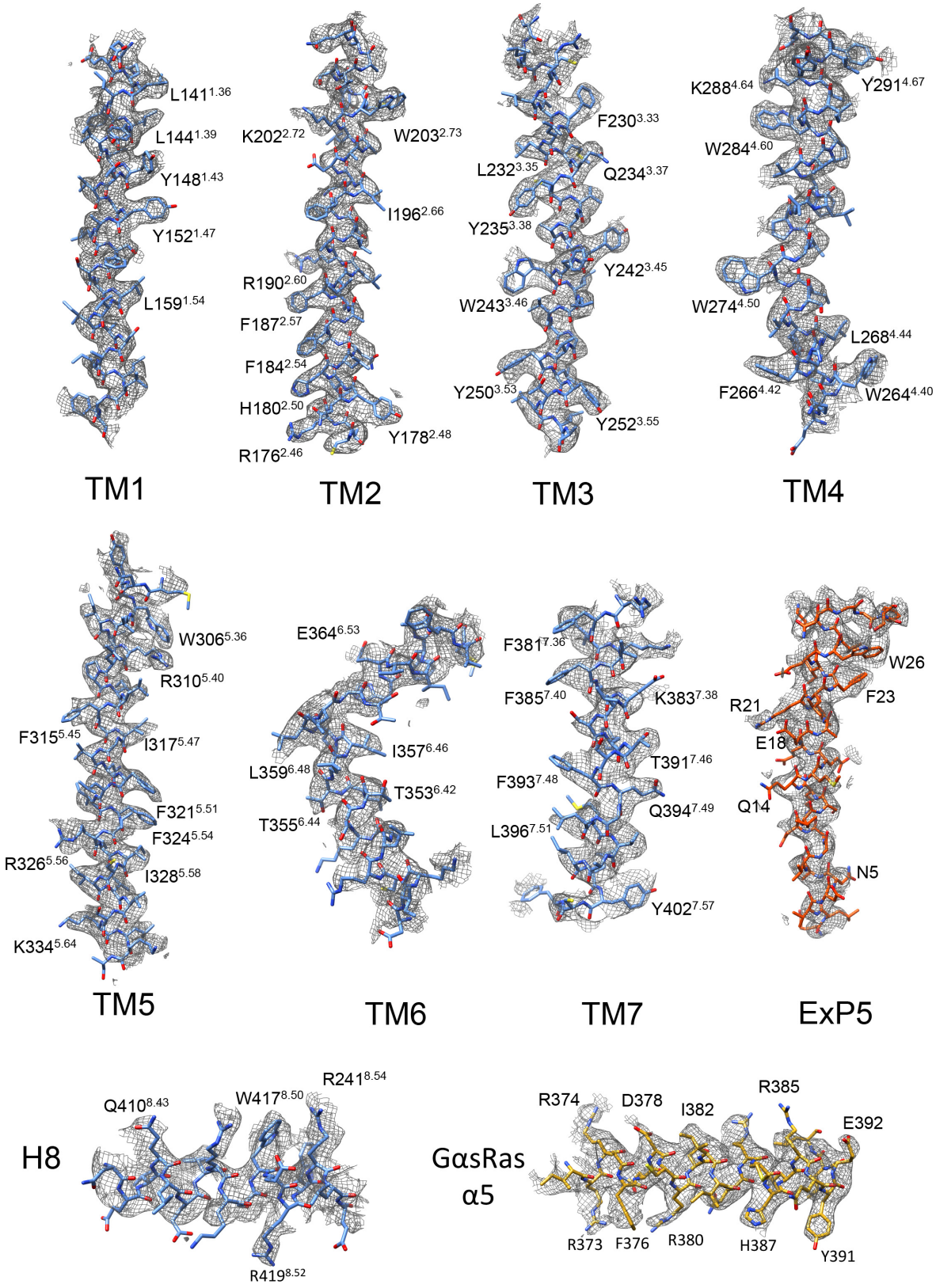

Extended Data Figure 3 | Atomic resolution model of the ExP5–GLP-1R–Gs heterotrimer in the cryo-EM density map. EM density map and model are shown for all seven transmembrane helices and H8 of the receptor, the ExP5 peptide and the α5α helix of the GαSα Ras-like domain. Bulky residues are highlighted. All transmembrane helices exhibit good density, with TM6—which is flexible—being the least well-resolved.

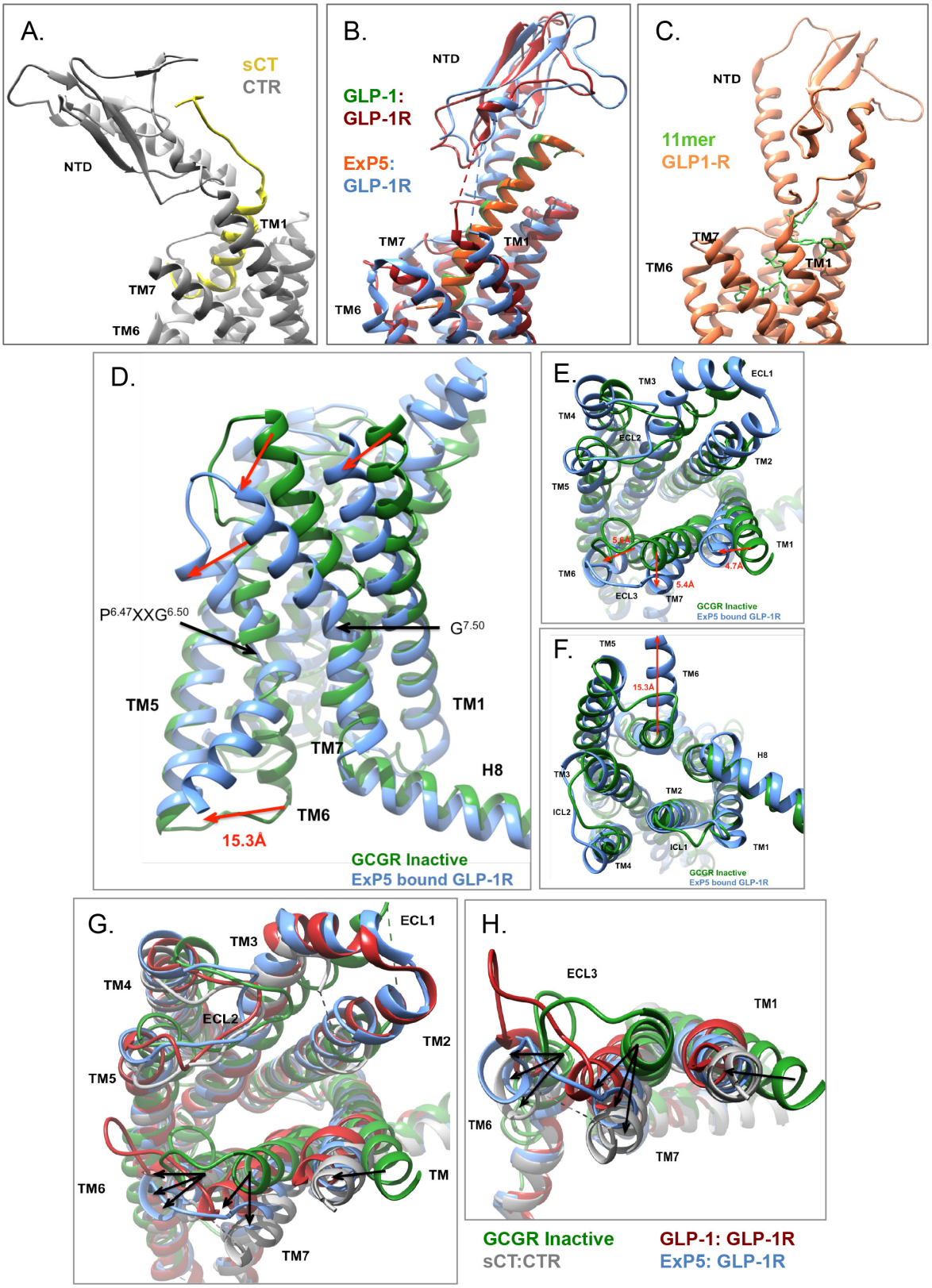

Extended Data Figure 4 | Comparison of class B GPCR structures. **a**–**c**, Agonist-bound full-length structures have distinct NTD orientations. **d**–**f**, Side view (**d**), extracellular view (**e**) and cytoplasmic view (**f**) of the conformational reorganization between inactive (GCGR, PDB 4L6R) and active structures (ExP5-bound GLP-1R). Distances are measured from Cα residues 1.33, 6.58, 7.35 and 6.35. Numbering uses the Wootten class B system. **g**–**h**, Superimposition of transmembrane domains from sCT–CTR–Gs (grey, PDB 5U27), GLP-1–GLP-1R–Gs (red, PDB 5VAI) and ExP5–GLP-1R–Gs with the inactive GCGR (green, PDB 4L6R). The largest differences in active structures relative to the inactive GCGR occur in TM1, TM6, TM7 and ECL3 (**h**), but the nature and extent of conformational change varies.

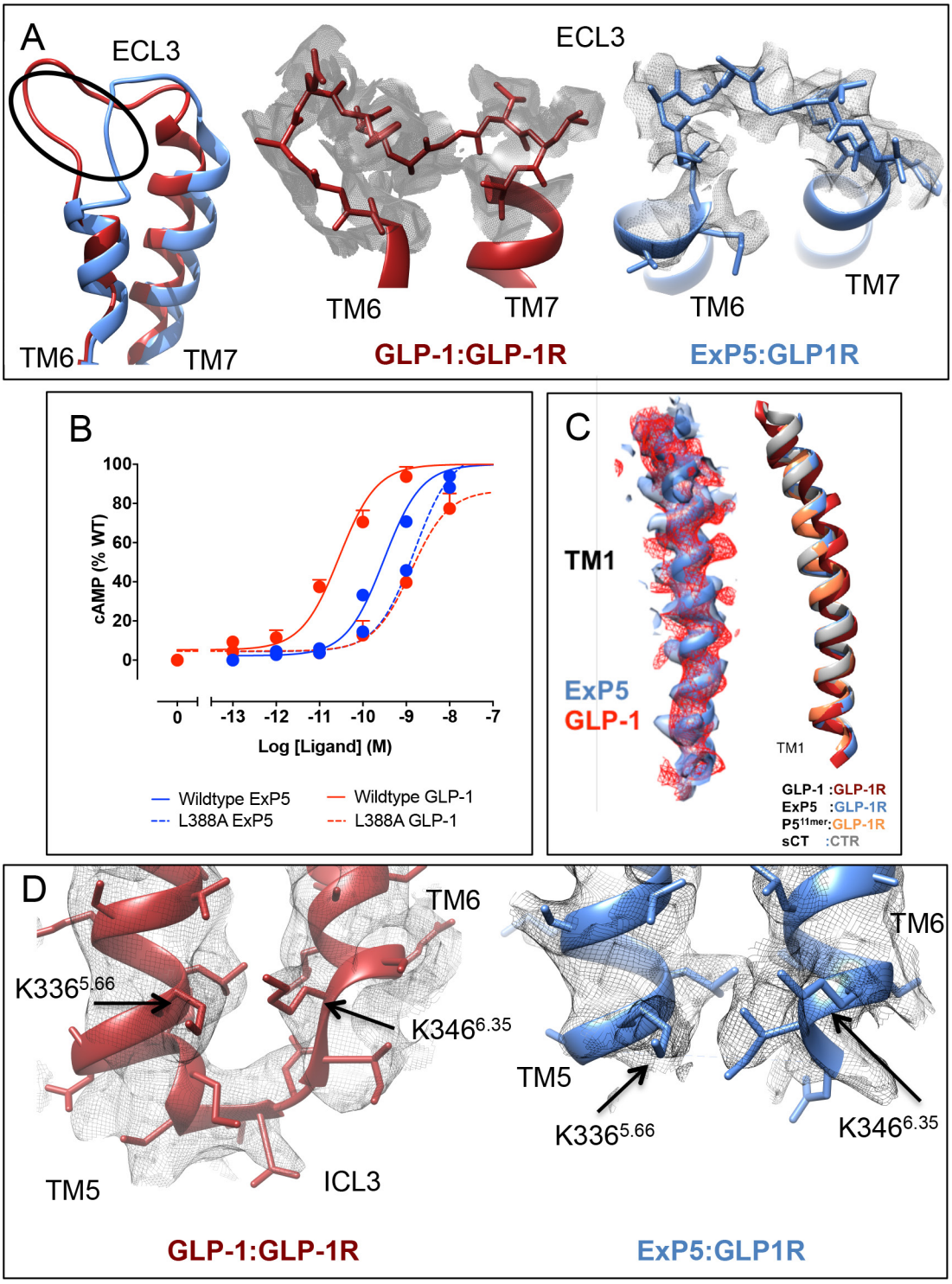

Extended Data Figure 5 | ECL3, TM7, TM1 and ICL3 may be associated with GLP-1R biased agonism. a, Conformational differences in GLP-1R ECL3 between ExP5-bound (blue) and GLP-1-bound (red) GLP-1R structures are supported by density in their respective cryo-EM maps. **b**, L388$^{7.43}$A affected the potency of GLP-1 mediated cAMP more than ExP5 (mean + s.e.m. of four independent experiments). **c**, Right, TM1 overlays from agonist-bound class B GPCR structures reveals a different conformation for GLP-1–GLP-1R. Left, TM1 model overlays of ExP5–GLP-1R and GLP-1–GLP-1R with their associated cryo-EM maps (GLP-1, red ribbon/mesh; ExP5, blue ribbon/surface) reveals limited differences in the TM1 backbone, but potentially distinct side-chain orientations. **d**, Left, ICL3 backbone conformation in GLP-1–GLP-1R (PDB 5VAI) is supported by density (EMD-3653). Limited density is observed for ICL3 (337–343) in ExP5–GLP-1R.

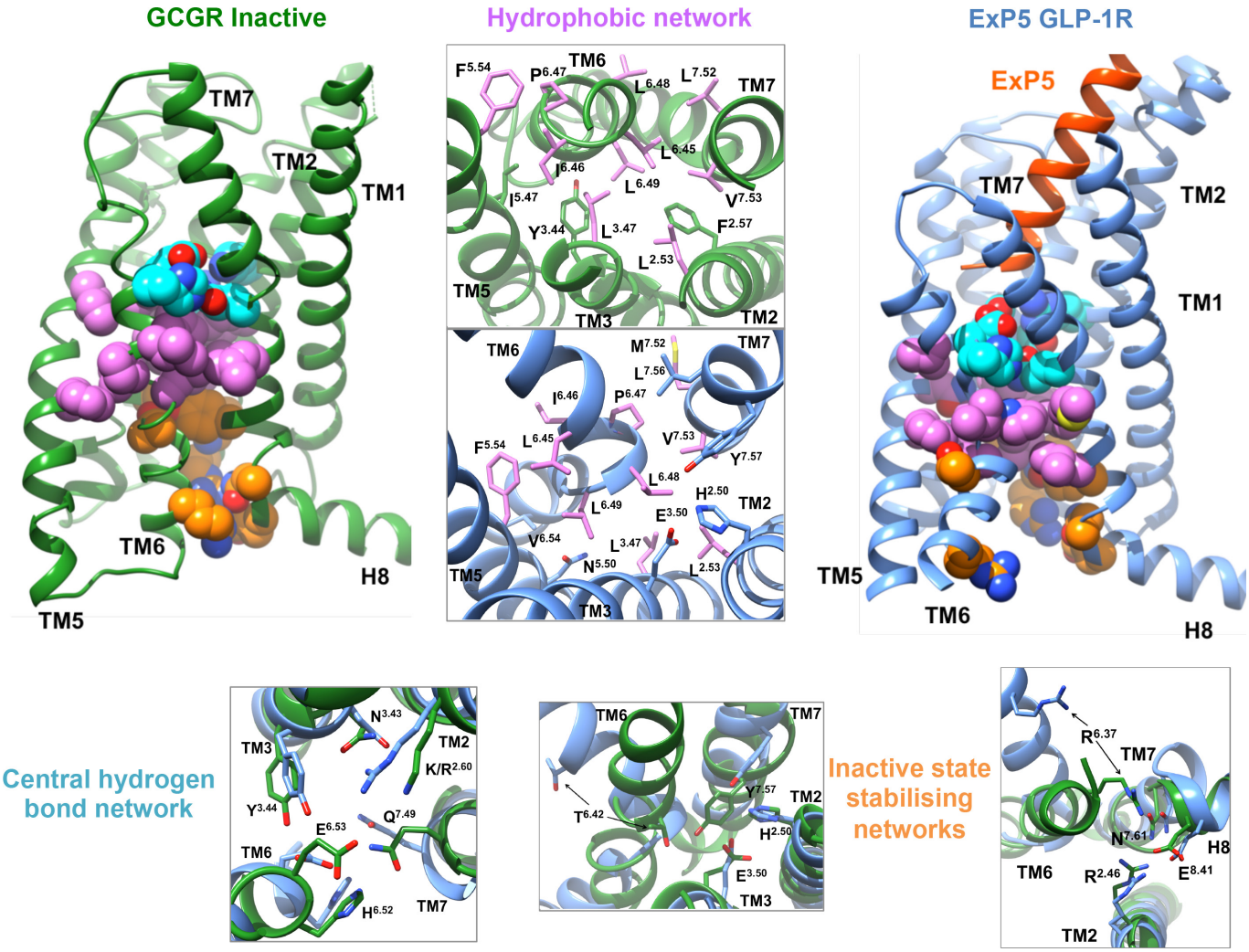

Extended Data Figure 6 | Rearrangement of conserved networks upon GLP-1R binding to ExP5. Comparison of conserved networks in the inactive (green, GCGR) and activated (blue, ExP5–GLP-1R–Gs) states; central polar network (cyan), cytoplasmic polar networks (orange) and hydrophobic residues (pink). Inactive state interactions are incompatible with peptide binding and reorganize on activation. Upper middle, major rearrangements within the hydrophobic network (top, inactive; bottom, activated); side chains involved in ground state stabilization in green, inactive and active state in pink and active state in blue. Lower left and lower right, reorganization of the central hydrogen bond network and cytoplasmic networks, respectively, where green is inactive and blue is active. Subscript, Wootten numbering. These conformational changes are detailed in Supplementary Video 1.

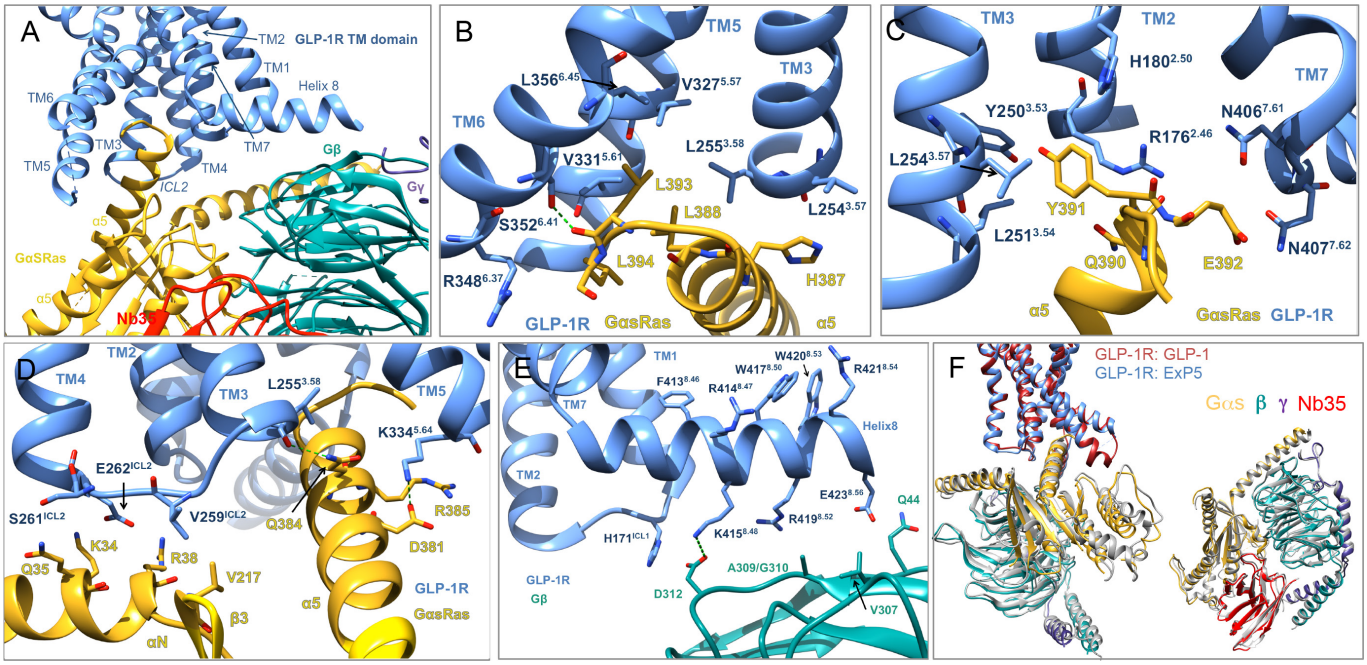

Extended Data Figure 7 | GLP-1R–G protein interactions. a, GLP-1R forms interactions with $G\alpha_s$Ras and Gβ. **b**–**e**, Receptor side chains (blue) within 4.5 Å of $G\alpha_s$ side chains (gold) or Gβ side chains (cyan). **b**–**d**, $G\alpha_s\alpha5$ forms polar and non-polar interactions with the cytoplasmic cavity formed by TM6 opening. Potential interactions also occur between $G\alpha_s\alpha N$ and ICL2 of GLP-1R. **e**, GLP-1R H8 aromatic residues embed within the detergent micelle and polar residues form direct interactions with Gβ. **f**, Left, the distinct engagement angle of $G\alpha_s\alpha5$ with the receptor (Fig. 3) results in an overall rotation of the $G\alpha_s$Ras,β,γ in ExP5–GLP-1R relative to GLP-1–GLP-1R. Right, overlaying $G\alpha_s$ from both structures reveals only minor differences in the G protein upon receptor engagement.

Extended Data Table 1 | Effects of extracellular loop 3 alanine mutants of human GLP-1R on agonist binding and cell surface expression

GLP-1R	Cell surface expression	Whole cell competition radioligand binding pK_i			cAMP Accumulation					
		GLP-1	Exendin-4	Exendin-P5	GLP-1		Exendin-4		Exendin-P5	
					pEC_{50}	E_{max}	pEC_{50}	E_{max}	pEC_{50}	E_{max}
Wild type	100 ± 3	8.81±0.04 -	8.97±0.07 -	9.61±0.45(0.18) 7.05±0.09	10.8±0.04	100±2	11.4±0.04	100±1	9.93±0.04	100±1
D372A	86 ± 4	9.62±0.47 (0.15)	9.29±0.56 (0.14) **7.40±0.21***	9.34±0.41 (0.24) 6.85±0.09	**8.95±0.10***	103±4	**10.1±0.09***	105±3	10.0±0.08	99±2
E373A	94 ± 7	9.80±0.39 (0.26)	9.67±0.42 (0.10) **7.41±0.15***	9.55±0.29 (0.22) 6.71±0.08	**8.45±0.08***	104±4	**9.3±0.09***	99±3	**9.25±0.08***	106±3
H374A	82 ± 8	8.87±0.14 -	8.87±0.09 -	9.94±0.52 (0.10) 7.24±0.13	10.9±0.07	102±2	11.6±0.08	99±2	10.1±0.07	93±2
R376A	92 ± 7	8.53±0.10 -	8.92±0.10 -	9.61±0.48 (0.15) 7.05±0.09	**10.3±0.09***	99±3	11.4±0.12	95±2	9.61±0.14	105±5
G377A	96 ± 3	**8.27±0.06***	9.12±0.25 (0.68) **7.29±0.21***	- 7.03±0.10	**9.9±0.08***	105±3	11.1±0.15	102±4	**9.14±0.15***	106±5
T378A	173 ± 11*	8.87±0.06	8.71±0.11	- 6.75±0.08	10.7±0.10	93±2	11.5±0.17	85±7	10.0±0.10	95±3
L379A	90 ± 6	**8.33±0.07***	**8.15±0.15***	9.61±0.49 (0.15) **6.63±0.11***	**9.74±0.13***	89±3	**10.5±0.20***	92±5	10.2±0.10	96±3
R380A	73 ± 5	**7.35±0.09***	**7.65±0.05***	- **6.65±0.04***	**7.74±0.07***	103±4	**8.81±0.08***	103±3	**8.21±0.11***	97±4
F381A	92 ± 5	8.97±0.06	8.94±0.05	9.22±0.51 (0.19) **6.32±0.15***	10.5±0.06	88±2	11.5±0.08	86±6	10.3±0.06	93±2
I382A	115 ± 6	8.92±0.06	8.91±0.06	9.71±0.51 (0.14) 6.79±0.12	10.9±0.12	99±3	11.3±0.09	95±2	10.2±0.12	102±4

Cell surface expression was determined through antibody detection of the N-terminal c-Myc epitope label and expressed as percentage of wild-type (WT) GLP-1R expression. Whole-cell competition radioligand binding data were analysed using either a one-site (a single pK_i) or a two-site binding curve (two pK_i values are reported with the fraction of receptors in the high affinity site reported in brackets) as determined by an *F*-test in Graphpad Prism. pK_i values represent the negative logarithm of the equilibrium dissociation constant (in molar) of agonist. Data were normalized to specific [^{125}I]-exendin(-9-39) binding. cAMP concentration response data were analysed using a three-parameter logistic curve to determine pEC_{50} and E_{max} values. pEC_{50} values represent the negative logarithm of agonist concentration that produces half maximal response. E_{max} values are maximal response as percentage of WT response. All values are expressed as mean ± s.e.m. of five independent experiments conducted in duplicate. Data were analysed using one-way analysis of variance and Dunnett's post-test. $^*P < 0.05$ (in comparison with WT response).

Extended Data Table 2 | Interactions between the GLP-1R and ExP5

ExP5	Peptide side chain density at Cβ	Peptide side chain density at Cγ	GLP-1R	Interaction
E1	yes	no	R310$^{5.40}$ A368$^{6.57}$	Hydrogen bond
L2	yes	yes	V237$^{3.40}$ I313$^{5.43}$	
V3	yes	N/A	L384$^{7.39}$ E387$^{7.42}$ L388$^{7.43}$ *T391$^{7.46}$*	
D4	no	no	Y152$^{1.47}$ V194$^{2.64}$ M233$^{3.36}$ *K197$^{2.67}$*	Potential H-bond Salt bridge
N5	yes	yes	Q234$^{3.37}$ W306$^{5.36}$	Hydrogen bond Hydrogen bond
A6	yes	N/A		
V7	yes	N/A	L384$^{7.39}$ L388$^{7.43}$	
G8	N/A	N/A		
G9	N/A	N/A		
D10	yes	no	R380$^{7.35}$	Salt bridge
L11	yes	no	L141$^{1.36}$ *Y145$^{1.40}$* *L201$^{2.71}$*	
S12	yes	N/A	T298^{ECL2} L201$^{2.71}$	
K13	yes	yes	R299^{ECL2} backbone	potential H-bond to the backbone
Q14	yes	yes	E138$^{1.33}$ L141$^{1.36}$	no side chain density for E138
M15	yes	yes	L201$^{2.71}$ K202$^{2.71}$ Y205$^{2.75}$ S206$^{2.76}$	
E16	yes	yes	Y205$^{2.75}$ R299^{ECL2} N32	Potential H-bond Salt bridge, Potential H-bond to the backbone
E17	yes	no	*Potentially TM1 stalk*	
E18	yes	yes	*Potentially TM1 stalk*	
A19	yes	N/A	Y205$^{2.75}$	
V20	yes	N/A	*V30^{NTD}* L32^{NTD} P90^{NTD}	
R21	yes	yes	*Potentially TM1 stalk*	
L22	yes	yes	*Q210^{ECL1}*	
F23	yes	yes	W214^{ECL1} *L32^{NTD}* *L35^{NTD}* *V36^{NTD}* W39^{NTD}	
I24	yes	yes	 V20^{NTD} Y69^{NTD} *L89^{NTD}* P90^{NTD} W91^{NTD}	
E25	yes	yes		
W26	yes	yes	H212^{ECL1} W214^{ECL1}	 π-stack
L27-S33			N-terminal interactions	

Residues in black are within 4 Å of the bound peptide. Residues in grey italics are within 4.5 Å of the bound peptide, but out of bonding distance and may form transient interactions. Residues in blue italics are within 4 Å in our model but there is no side-chain density in the cryo-EM map.

Extended Data Table 3 | Interactions formed between class B receptor and Gs heterotrimeric Gs proteins

G protein subunit	G protein Residue no	GLP-1R (ExP5 bound)	GLP-1R (GLP-1 bound) PDB: 5VAI	CTR (sCT bound) PDB:5UZ7
GαRas α5	R380	*F257^{ICL2}*	L256$^{2.59}$bb	K326$^{6.54}$
	D381	K334$^{5.64}$	K334$^{5.64}$	
	I383	*S258^{ICL2}*		V252^{ICL2}
	Q384	L255$^{2.58}$bb K334$^{5.64}$	L255$^{2.58}$bb K334$^{5.64}$	L248$^{2.58}$bb K326$^{5.64}$
	R385	K334$^{5.64}$ bb	K334$^{5.64}$bb	K326$^{5.64}$
	H387	L254$^{3.57}$ L255$^{2.58}$	L254$^{3.57}$	L247$^{3.57}$
	L388	L255$^{2.58}$ V331$^{5.61}$ *K334$^{5.64}$*	V331$^{5.61}$	L323$^{5.61}$
	Q390	R176$^{2.46}$	R176$^{2.46}$ E408$^{8.41}$	R180$^{2.46}$
	Y391	*H180$^{2.50}$* Y250$^{3.53}$ L251$^{3.54}$ ***L254$^{3.57}$***	H180$^{2.50}$ L359$^{6.48}$ L356$^{6.45}$ L251$^{3.54}$	Y253^{ICL2} L244$^{3.54}$
	E392	*N406$^{7.61}$* N407$^{7.62}$	N406$^{7.61}$ V405$^{7.60}$bb L401$^{7.56}$bb	***C394$^{7.60}$bb*** ***N396$^{7.62}$***
	L393	S352$^{6.41}$bb L356$^{6.45}$ ***V327$^{5.57}$*** *V331$^{5.61}$*	*S352$^{6.41}$* L356$^{6.45}$ T353$^{6.42}$	L348$^{6.45}$
	L394	*V331$^{5.61}$* *R348$^{6.37}$ (to L394 backbone)*	*L339$^{5.59}$*	M327$^{5.65}$
GαRas αN	Q35	S261^{ICL2}	S261^{ICL2} E262^{ICL2}	
	R38	E262^{ICL2}		
	Q31	Q263^{ICL2} (not support density)	Q263^{ICL2}	
	K34	*E262^{ICL2}*	Q263^{ICL2}	
GαRas β3	V217	V259^{ICL2}		
GαRas α4	R385	*(N338 not resolved in cryo EM map but likely conserved)*	N338^{ICL3}	
Gβ	D312	H171^{ICL1} K415$^{8.48}$	H171^{ICL1} K415$^{8.48}$	R404$^{8.48}$
	A309/G310 (backbone)	R419$^{8.52}$	R419$^{8.52}$	Q408$^{8.52}$
	Q44	*E423$^{8.56}$*		Q415$^{8.60}$

All receptor residues within 4 Å (4.5 Å in non-bold italics) of G protein that were evident in the cryo-EM maps of the sCT–CTR–Gs, GLP-1–GLP-1R–Gs and ExP5–GLP-1R–Gs complexes are listed. Residues in red are conserved interactions between the three structures, those in blue are conserved between the two GLP-1R structures and those in black are unique in the different structures (bb indicates backbone interactions).

nature research

Corresponding author(s): Patrick M. Sexton, Denise Wootten

☐ Initial submission ☒ Revised version ☐ Final submission

Life Sciences Reporting Summary

Nature Research wishes to improve the reproducibility of the work that we publish. This form is intended for publication with all accepted life science papers and provides structure for consistency and transparency in reporting. Every life science submission will use this form; some list items might not apply to an individual manuscript, but all fields must be completed for clarity.

For further information on the points included in this form, see Reporting Life Sciences Research. For further information on Nature Research policies, including our data availability policy, see Authors & Referees and the Editorial Policy Checklist.

Experimental design

1. Sample size

Describe how sample size was determined. Sample size calculation was not required

2. Data exclusions

Describe any data exclusions. No data were excluded

3. Replication

Describe whether the experimental findings were reliably reproduced. Experimental findings were reliably reproduced

4. Randomization

Describe how samples/organisms/participants were allocated into experimental groups. Randomization was not required

5. Blinding

Describe whether the investigators were blinded to group allocation during data collection and/or analysis. Blinding was not required

Note: all studies involving animals and/or human research participants must disclose whether blinding and randomization were used.

6. Statistical parameters

For all figures and tables that use statistical methods, confirm that the following items are present in relevant figure legends (or in the Methods section if additional space is needed).

n/a	Confirmed
☐	☒ The exact sample size (*n*) for each experimental group/condition, given as a discrete number and unit of measurement (animals, litters, cultures, etc.)
☒	☐ A description of how samples were collected, noting whether measurements were taken from distinct samples or whether the same sample was measured repeatedly
☐	☒ A statement indicating how many times each experiment was replicated
☐	☒ The statistical test(s) used and whether they are one- or two-sided (note: only common tests should be described solely by name; more complex techniques should be described in the Methods section)
☒	☐ A description of any assumptions or corrections, such as an adjustment for multiple comparisons
☐	☒ The test results (e.g. *P* values) given as exact values whenever possible and with confidence intervals noted
☐	☒ A clear description of statistics including central tendency (e.g. median, mean) and variation (e.g. standard deviation, interquartile range)
☐	☒ Clearly defined error bars

See the web collection on statistics for biologists for further resources and guidance.

Software

Policy information about availability of computer code

7. Software

Describe the software used to analyze the data in this GraphPad Prism, ImageJ, Motioncor2, Gctf, Gautomatch, EMAN2, Relion 2.03,

study.	PHENIX, MolProbity, COOT, Pymol, UCSF Chimera

For manuscripts utilizing custom algorithms or software that are central to the paper but not yet described in the published literature, software must be made available to editors and reviewers upon request. We strongly encourage code deposition in a community repository (e.g. GitHub). *Nature Methods* guidance for providing algorithms and software for publication provides further information on this topic.

Materials and reagents

Policy information about availability of materials

8. Materials availability

Indicate whether there are restrictions on availability of unique materials or if these materials are only available for distribution by a for-profit company.	There are no restriction

9. Antibodies

Describe the antibodies used and how they were validated for use in the system under study (i.e. assay and species).	All antibodies were used for Western blot analysis and have been validated. rabbit anti-Gs C-18 antibody (cat no sc-383), Santa Cruz mouse Penta-His antibody (cat no 34660), QIAGEN 680RD goat anti-mouse antibody (LI-COR) 800CW goat anti-rabbit antibody (LICOR)

10. Eukaryotic cell lines

a. State the source of each eukaryotic cell line used.	Cells used in assays were obtained from ATCC
b. Describe the method of cell line authentication used.	No authentication required
c. Report whether the cell lines were tested for mycoplasma contamination.	Cell lines were tested and are free from mycoplasma contamination
d. If any of the cell lines used are listed in the database of commonly misidentified cell lines maintained by ICLAC, provide a scientific rationale for their use.	Cells are not listed in the database

Animals and human research participants

Policy information about studies involving animals; when reporting animal research, follow the ARRIVE guidelines

11. Description of research animals

Provide details on animals and/or animal-derived materials used in the study.	Not applicable

Policy information about studies involving human research participants

12. Description of human research participants

Describe the covariate-relevant population characteristics of the human research participants.	Not applicable